

Infrared and Raman spectra of LiV_2O_5 single crystals

Z.V.Popović^a, R. Gajić^b, M.J.Konstantinović^c, R. Provoost^a, V. V. Moshchalkov^a,
A.N.Vasil'ev^d, M.Isobe^e and Y.Ueda^e

^a *Laboratorium voor Vaste-Stoffysica en Magnetism, Katholieke Universiteit Leuven,
Celestijnenlaan 200 D, Leuven 3001, Belgium*

^b *Institute of Physics, 11080 Belgrade, P.O.Box 86, Yugoslavia*

^c *Max-Planck-Institut für Festkörperforschung, Heisenbergstr. 1, D-70569 Stuttgart, Germany*

^d *Low Temperature Physics Department, Moscow State University, 119899 Moscow, Russia*

^e *Institute for Solid State Physics, The University of Tokio, 7-22-1 Roppongi, Minato-ku, Tokio
106, Japan*

Abstract

The phonon dynamics of LiV_2O_5 single crystals is studied using infrared and Raman spectroscopy techniques. The infrared-active phonon frequencies and dielectric constants are obtained by oscillator fitting procedure of the reflectivity data measured at room temperature. The Raman scattering spectra are measured at room temperature and at $T=10$ K in all nonequivalent polarized configurations. The assignment of the phonons is done by comparing the infrared and Raman spectra of LiV_2O_5 and NaV_2O_5 . The factor-group-analysis of the LiV_2O_5 crystal symmetry and of its constituent layers is performed to explain the symmetry properties of the observed modes. We concluded that layer symmetry dominates in the vibrational properties of this compound.

I. INTRODUCTION

During the past several years low dimensional quantum spin systems such as the spin-Peierls, spin-ladder and an antiferromagnetic Heisenberg linear chain systems have attracted much attention¹. The vanadate family of AV_2O_5 oxides ($A = \text{Li, Na, Cs, Mg and Ca}$), which have common $V^{4+}O_5$ square pyramids in the structure, have demonstrated a variety of the low dimensional quantum spin phenomena: charge-ordering transition in NaV_2O_5 ², spin-gap behavior in $Ca(\text{Mg})V_2O_5$ ³ and CsV_2O_5 ⁴ and typical 1-D behavior without spin gap in LiV_2O_5 ⁴. The magnetic susceptibility data, fitted in the framework of the Bonner-Fisher model with the exchange interaction $J=308 \text{ K}$ ⁴, suggest that the magnetic properties of this system can be described using homogenous Heisenberg antiferromagnetic linear chain model. The nuclear magnetic resonance (NMR) measurements showed the formation of the staggered spin configurations due to the existence of the finite-size effect⁵.

However, in spite of good understanding of the magnetic properties, the study of the vibrational properties of LiV_2O_5 is of a great importance because of the still puzzling interplay between the charge and the magnetic ordering in NaV_2O_5 ⁶. Thus, in this work we present the polarized far-infrared (FIR) reflectivity as well as the Raman scattering spectra of LiV_2O_5 single crystals. The $16A_g$, $7B_{1g}$, $6B_{3g}$, $9B_{3u}$, and $5B_{2u}$ symmetry modes are experimentally observed. The assignment of the vibrational modes is done by comparing the phonons in LiV_2O_5 and NaV_2O_5 . Furthermore, our spectra demonstrate the dominance of the layer symmetry in LiV_2O_5 .

II. EXPERIMENT

The present work was performed on single crystal plates with dimensions typically about $1 \times 4 \times 0.5 \text{ mm}^3$ in the **a**, **b**, and **c** axes, respectively. The details of sample preparation were published elsewhere⁴. The infrared measurements were carried out with a BOMEM DA-8 FIR spectrometer. A DTGS pyroelectric detector was used to cover the wave number region from 100 to 700 cm^{-1} ; a liquid nitrogen cooled HgCdTe detector was used from 500 to 1500 cm^{-1} . Spectra were collected with 2 cm^{-1} resolution, with 1000 interferometer scans added for each spectrum. The Raman spectra were measured in the backscattering configuration using micro-Raman system with DILOR triple monochromator including liquid nitrogen cooled CCD-detector. An Ar-ion laser was used as an excitation source.

III. RESULTS AND DISCUSSION

LiV_2O_5 has an orthorhombic unit cell⁷ with parameters $a=0.9702 \text{ nm}$, $b=0.3607 \text{ nm}$, $c= 1.0664 \text{ nm}$, $Z=4$ and space group $Pnma (D_{2h}^{16})$. Each vanadium atom is surrounded by five oxygen atoms, forming VO_5 pyramids. These pyramids are mutually connected via common edges to form zigzag chains along the **b**-direction. Such a crystalline structure is characterized by two kinds of vanadium double chains along the **b**-axis. One is magnetic V^{4+} ($S=1/2$) and the other one is nonmagnetic V^{5+} ($S=0$) chain. These chains are linked by corner sharing to form layers in (001) - plane, Fig. 1 (a). The Li atoms are situated between these layers, as shown in Fig. 1.1.(b). The LiV_2O_5 unit cell consists of four formula

units comprising 32 atoms in all (Fig. 1). The site symmetry of all atoms in Pnma space group is C_s . The factor-group-analysis (FGA) yields⁸:

(Li, V₁, V₂, O₁, O₂, O₃, O₄, O₅) (C_s):

$$\Gamma = 2A_g + A_u + B_{1g} + 2B_{1u} + 2B_{2g} + B_{2u} + B_{3g} + 2B_{3u},$$

Summarizing these representations and subtracting the acoustic ($B_{1u} + B_{2u} + B_{3u}$) and silent ($8A_u$) modes, we obtained the following irreducible representations of LiV₂O₅ vibrational modes of Pnma space group:

$$\Gamma = 16A_g(\text{aa,bb,cc}) + 8B_{1g}(\text{ab}) + 16B_{2g}(\text{ac}) + 8B_{3g}(\text{bc}) + 15B_{1u}(\mathbf{E}||\mathbf{c}) + 7B_{2u}(\mathbf{E}||\mathbf{b}) + 15B_{3u}(\mathbf{E}||\mathbf{a})$$

Thus, 48 Raman and 37 infrared active modes are expected to show up in the LiV₂O₅ spectra. The room temperature polarized far-infrared reflectivity spectra of LiV₂O₅ are given in Fig. 2. The open circles are the experimental data and the solid lines represent the spectra computed using a four-parameter model for the dielectric constant⁹.

$$\epsilon = \epsilon_\infty \prod_{j=1}^n \frac{\omega_{LO,j}^2 - \omega^2 + i\gamma_{LO,j}\omega}{\omega_{TO,j}^2 - \omega^2 + i\gamma_{TO,j}\omega} \quad (1)$$

where $\omega_{LO,j}$ and $\omega_{TO,j}$ are longitudinal and transverse frequencies of the j^{th} oscillator, $\gamma_{LO,j}$ and $\gamma_{TO,j}$ are their corresponding dampings, and ϵ_∞ is the high-frequency dielectric constant. The static dielectric constant, given in Table I, is obtained using the generalized Lyddane-Sachs-Teller relation $\epsilon_0 = \epsilon_\infty \prod_{j=1}^n \omega_{LO,j}^2 / \omega_{TO,j}^2$.

The best-oscillator-fit parameters are listed in Table I. The agreement between observed and calculated reflectivity spectra is rather good. For the $\mathbf{E}||\mathbf{a}$ polarization, nine oscillators with TO frequencies at about 202, 243, 255, 340, 397, 545, 724, 948, 1006 cm^{-1} are clearly seen. In the $\mathbf{E}||\mathbf{b}$ polarization (Fig. 2 (b)) five oscillators at 180, 255, 323, 557 and 595 cm^{-1} are observed. We failed to obtain useful signal for $\mathbf{E}||\mathbf{c}$ spectra because of the very small thickness (\mathbf{c} -axis) of the sample. The room and the low temperature Raman spectra of LiV₂O₅, for parallel and crossed polarizations, are given in Fig. 3. The spectra for parallel polarizations consist of A_g symmetry modes. Thirteen modes at 100, 123, 172, 209, 328, 374, 398, 528, 550, 639, 725, 965 and 989 cm^{-1} are clearly seen for the (aa) polarization, two additional modes at 197 and 456 cm^{-1} for the (bb) polarization and one additional mode at 267 cm^{-1} for the (cc) polarization. For the crossed (ab) polarization seven Raman active B_{1g} symmetry modes at 168, 250, 270, 333, 546, 646 and 737 cm^{-1} are found. In the case of the (bc) polarization, six B_{3g} symmetry modes were observed with almost the same frequencies as B_{1g} modes. The Raman spectra for (ac) polarization is given in Fig. 3 (f). For this polarization (B_{2g} symmetry) we could not resolve any new mode. Namely, all modes observed for this polarization have been already seen in parallel or in other crossed polarizations, probably because of low-quality of the (010) surface. The frequencies of all observed Raman active modes are given in Table II.

We will first consider the Raman spectra shown in Fig. 3. From the 16 A_g , 8 B_{1g} , 8 B_{3g} and 16 B_{2g} modes predicted by FGA of LiV₂O₅, we clearly observe 16 A_g , 7 B_{1g} , and 6 B_{3g} modes. The missing modes seem to be of a very weak intensity. The (ac) polarized spectra (Fig. 3 (f)) consist mostly of A_g modes (and some B_{1g}). The appearance of B_{1g} and B_{3g} symmetry modes at the same frequencies lead us to consider the crystal structure of this oxide once again. The LiV₂O₅ crystal is a layer crystal (see Fig. 1 (b)). The vibrational properties of such crystals demonstrate the dominance of the layer symmetry^{9,10}. The unit

cell of LiV_2O_5 consists of two layers with 16 atoms in all. The full symbol of space group is $P 2_1/n 2_1/m 2_1/a$. The first symbol represents 2_1 -screw axis along \mathbf{a} -axis followed by diagonal glide plane (n) perpendicular to \mathbf{a} -axis with translation $(b+c)/2$; the second symbol is the 2_1 -screw axis parallel to \mathbf{b} -axis with mirror plane perpendicular to it and third symbol means 2_1 -screw axis parallel to \mathbf{c} -axis with glide plane perpendicular to \mathbf{c} -axis with translation of $a/2$ (see the lower part of Fig. 4). If we consider only one layer we break the periodicity in the direction perpendicular to the layer. As a consequence, there are no more symmetry operations along the \mathbf{a} - and \mathbf{c} -axes. Now we should consider the layer symmetry in terms of diperiodic groups¹¹ rather than triperiodic space groups. We found four operation of layer symmetry, Fig. 4:

- 1, identity
- 2_1 , twofold screw axis parallel to the \mathbf{b} -axis
- $\bar{1}$, center of symmetry located between VO_5 pyramids
- m, mirror plane perpendicular to the \mathbf{b} -axis.

The DG15 diperiodic group is the only symmetry operation group of 80 that has these symmetry operations. The full symbol of this diperiodic group is $P 1 2_1/m 1$. This group is isomorphic with the C_{2h}^2 ($P2_1/m$) space group (second setting)¹². All atoms are in symmetry position (e) of this space group (with C_s point symmetry). The normal mode distribution for the layer is

$$\Gamma = 16A_g (\text{xx,yy,zz, xz}) + 8B_g (\text{xy, yz}) + 8A_u (\mathbf{E}||\mathbf{y}) + 16B_u (\mathbf{E}||\mathbf{x}, \mathbf{E}||\mathbf{z})$$

The compatibility diagram, relating the layer and the crystal vibration of LiV_2O_5 , together with the schematic representation of the layer and the crystal symmetry operations as well as the experimental conditions for the observation of the optical modes, are given in Fig. 4. According to Fig. 4 the A_g modes for the layer symmetry appear for parallel and for (ac) crossed polarization and the B_{1g} and B_{3g} modes of crystal symmetry merge into B_g modes of the layer symmetry. These facts are fully in agreement with our Raman spectra, Fig. 3. Thus, we can conclude that the vibrational properties of crystal are predominantly due to vibrational properties of the layer. As we already mentioned, the size of samples in (010) plane and worse quality of this surface do not allow us to check this conclusion also by infrared spectroscopy.

By comparing the LiV_2O_5 spectra with the corresponding spectra and the lattice dynamics of NaV_2O_5 ^{13,14} we analyze the LiV_2O_5 phonon properties. The basic building blocks of LiV_2O_5 crystal structure are VO_5 pyramids which are mutually connected by edge to build the chains. Such chains are also present in NaV_2O_5 . The difference between crystal structures of Na- and Li- vanadate is illustrated in Fig. 5. In NaV_2O_5 there is only one vanadium site while in LiV_2O_5 two nonequivalent vanadium atom positions are present. Besides that, the $\text{V}_1\text{-O-V}_2$ angle in LiV_2O_5 is smaller (120°) than in NaV_2O_5 (140°). Distance between atoms in VO_5 pyramids does not differ significantly in Li- and Na- vanadates. This produces only a small frequency shift of the corresponding modes in these compounds. The existence of the two different VO_5 chains with nearly the same inter-atomic distance can produce the appearance of mode doublets. Raman spectra for (aa) and (bb) polarizations of both compounds are shown in Fig. 5. As it can be seen from Fig. 5, each mode of NaV_2O_5 in the bond stretching region (above 450 cm^{-1}) appears as a doublet in LiV_2O_5 . The highest intensity mode in NaV_2O_5 originates from V-O_1 bond stretching vibration. The distance between these atoms in Na-vanadate is 1.62 \AA . In Li vanadate there are two such bonds,

one longer bond 1.65 \AA ($V_1\text{-O}_3$) and one slightly shorter 1.61 \AA ($V_2\text{-O}_2$) than $V\text{-O}_1$ bond in Na-vanadate. Thus, we can expect the appearance of two modes with frequencies higher and lower than the Na $V\text{-O}_1$ bond stretching frequency. In fact, two modes are observed in Fig. 5 at lower and higher frequency than Na $V\text{-O}_1$ mode. Applying the same analysis to the another doublet in bond stretching energy region we conclude that $528/550 \text{ cm}^{-1}$ modes originate from $V_1\text{-O}_4$ ($V_2\text{-O}_5$) bond stretching vibration. This doublet corresponds to the mode at 534 cm^{-1} of NaV_2O_5 .

Similar non - phononic broad structure, observed in Na - vanadate for (aa) polarization at about 640 cm^{-1} (see Fig. 5), is found in LiV_2O_5 as a doublet at about $639/725 \text{ cm}^{-1}$. There are several scenarios to explain this structure¹⁴. First, electric dipole transitions between split crystal field levels, second two-magnon scattering, and third possible electron-phonon coupled modes observed in antiferromagnets. In the case of NaV_2O_5 the wide structure shifts to lower energy upon cooling¹⁵. Fischer *et al.*¹⁴ concluded that such kind of behavior comes from electron-phonon coupling like in antiferromagnetic FeCl_2 ¹⁶. The opposite frequency shift vs. temperature of wide structure maximum in NaV_2O_5 then in FeCl_2 is connected with the strong spin fluctuations in low dimensions¹⁴.

Two-magnon excitations lead to broad band structures in Raman scattering spectra. The very recent neutron scattering measurements¹⁷ of LiV_2O_5 show antiferromagnetic periodicity along the b-axis (chain direction). These results suggests that LiV_2O_5 can be regarded as a collection of independent $S=1/2$ AF linear chains with zone boundary energy of $42 \pm 3 \text{ meV}$. The frequencies of observed modes ($640/725 \text{ cm}^{-1}$) are comparable with the values of exchange coupling energy $J=308 \text{ K}$ ($3J=640 \text{ cm}^{-1}$) and zone boundary energy range ($2E_{ZB}= 628\text{-}724 \text{ cm}^{-1}$), respectively. However, the polarization selection rules allow the appearance of modes for polarization of incident and scattered light parallel to the dominant exchange path (b-axis direction). Because we observed broad modes only for (aa) and (cc) polarization and there is no frequency shift of these modes to higher energies by lowering of the temperature we concluded that two-magnon scenario is not realistic.

Finally, we consider the appearance of these modes as crystal field induced¹⁸. These transitions between different crystal field levels should be discrete, and no significant frequency shift vs. temperature can be expected. This is in accordance with our spectra given in Fig.3. The appearance of two peaks can be understood due to existence of two structurally different strongly deformed VO_5 pyramids.

The mode at 788 cm^{-1} is probably IR active LO mode (790 cm^{-1} , see Table I) but its appearance is not understood at the moment.

The modes at frequencies below 450 cm^{-1} originate from bond bending vibrations. In the Na-vanadate the $V\text{-O}_3\text{-V}$ bending mode appears at 448 cm^{-1} . The corresponding mode in Li-vanadate could be the one at 374 cm^{-1} . Note that, the frequency of this mode is about 16 % lower than in Na-vanadate, as a consequence of the change of the bond-bending force constant. We make an approximate estimation for the change of the bond-bending force constant by scaling the frequency as the square root of the force constant, and assuming a scaling of the force constants as R^{-6} (R is the bond length)¹⁹. Similarly, scaling of the phonon frequency for the bond stretching mode is R^{-3} . In our case the $R(\text{O-V-O})_{\text{Na}}/R(\text{O-V-O})_{\text{Li}}$ is 0.98. This parameter can produce the decrease of the phonon frequency of only 5 %. The remaining part of frequency decrease probably comes from modification of bond-bending force constant due to redistribution of the electron density²⁰. Namely, according to

Refs.^{21,22} the electrons in NaV_2O_5 are located in a V-O₃-V molecular orbital. This is not the case in LiV_2O_5 where the electrons are located in V^{4+} chains.

The highest intensity mode for (bb) polarization in Li sample is the mode at 328 cm^{-1} . This mode originates from O-V-O bending vibrations as the highest intensity (bb) polarized mode in Na-sample. The broad structure at about 398 cm^{-1} seems to correspond to Li vibration. If we consider mass effect only, the replacement of heavier Na atoms with lighter Li produces the shift of corresponding mode towards higher frequency according to $(\omega_{\text{Na}}=179\text{ cm}^{-1}) \times (m_{\text{Na}}/m_{\text{Li}})^{1/2} = 326\text{ cm}^{-1}$, which is not too far from the observed mode. Besides, the Li-O vibrations are expected²³ at about 390 cm^{-1} . The pair of modes at $172/209\text{ cm}^{-1}$ originates from O-V-O bending vibration, and the pair of lowest frequency modes at $100/123\text{ cm}^{-1}$ represents chain rotation modes.

The similar analysis could be conducted for $\text{B}_{1(3)g}$ modes. Namely, the modes at 646 and 737 cm^{-1} are $\text{V}_1\text{-O}_4$ and $\text{V}_2\text{-O}_5$ bond stretching vibrations; the three modes at 250 , 270 and 333 cm^{-1} are bond bending vibrations, and the lowest frequency mode at 168 cm^{-1} represents chain rotation mode. We should mention that similar mode exists in NaV_2O_5 for crossed polarization too.

Identification of the infrared modes, obtained by comparison with IR spectra and lattice dynamics of NaV_2O_5 is given in Table I and we do not repeat it here again.

In conclusion, we have measured the infrared and Raman spectra of LiV_2O_5 . The assignment of the phonons is done by comparing the infrared and Raman spectra of LiV_2O_5 and NaV_2O_5 . The factor-group-analysis of the LiV_2O_5 crystal symmetry and of its constituent layers is performed to explain the symmetry properties of the observed modes. Finally, our spectra demonstrate the dominance of the layer symmetry in LiV_2O_5 .

Acknowledgments

Z.V.P. acknowledges support from the Research Council of the K.U. Leuven and DWTC. The work at the K.U. Leuven is supported by Belgian IUAP and Flemish FWO and GOA Programs. MJK thanks Roman Herzog - AvH for partial financial support.

REFERENCES

- ¹ E. Dagotto and T. M. Rice, *Science* **271**, 618 (1996).
- ² M. Isobe and Y. Ueda, *J.Phys. Soc. Jpn.* **65**, 1178 (1996).
- ³ H. Iwase, M. Isobe, Y. Ueda and H. Yasuoka, *J. Phys. Soc. Jpn.* **65**, 2397 (1996).
- ⁴ M. Isobe and Y. Ueda, *J.Phys. Soc. Jpn.* **65**, 3142 (1996).
- ⁵ N. Fujiwara, H Yasuoka, M. Isobe and Y. Ueda, *Phys. Rev. B* **58**, 11134 (1998).
- ⁶ M.J.Konstantinović, Z.V.Popović, A. N. Vasil'ev, M. Isobe and Y. Ueda *Solid State Commun.* **112**, 397 (1999).
- ⁷ D. N. Anderson and R. D. Willett, *Acta Cryst. B* **27**, 1476 (1971).
- ⁸ D. L. Rousseau, R. P Bauman, S.P.S. Porto, *J. Raman Spectrosc.* **10**, 253 (1981).
- ⁹ Z. V. Popović, *Phys. Rev. B* **32**, 2382 (1985).
- ¹⁰ R. Zallen, M. L. Slade, and A. T. Ward, *Phys. Rev. B* **3**, 4257 (1971); T. J. Wieting, *Solid State Commun.*, **12**, 931 (1973); T. J. Wieting and J. L. Verble, *Phys. Rev. B* **5**, 1473 (1972).
- ¹¹ E. A. Wood, *The 80 Diperic Groups in Three Dimensions*, Bell Telephone System Technical Monograph No. 4680, 1964 (unpublished).
- ¹² *International Tables for X-ray Crystallography* (1969), Vol.I, Birmingham, Kynoch Press.
- ¹³ Z. V. Popović, M. J. Konstantinović, R. Gajić, V. Popov, Y. S. Raptis, A. N. Vasil'ev, M. Isobe and Y. Ueda, *Solid State Commun.* **110**, 381 (1999).
- ¹⁴ M. Fischer, P. Lemmens, G. Els, G. Güntherodt, E. Ya. Sherman, E. Morre, C. Geibel, and F. Steglich, *Phys. Rev. B.* **60** 7284 (1999).
- ¹⁵ M. J. Konstantinović, Z. V. Popović, T. Ruf, M. Cardona, A. N. Vasil'ev, M. Isobe and Y. Ueda, *Phys. Stat. Sol. (b)* **215**, 661 (1999).
- ¹⁶ D. J. Lockwood, in *Light scattering in Solids III*, Vol. 51 of *Topics in Applied Physics*, edited by M. Cardona and G. Güntherodt (Springer Verlag, Berlin, 1982), p.59.
- ¹⁷ Y. Takeo, T. Yosihama, M. Nishi, K. Nakajama, K. Kakurai, M. Isobe, and Y. Ueda, *J. Phys. Chem. Solids.*, **60**, 1145 (1999).
- ¹⁸ S. A. Golubchik, M. Isobe, A. N. Ivlev, B. N. Mavrin, M. N. Popova. A. B. Sushkov, Y. Ueda, A. N. Vasil'ev, *J.Phys. Soc. Japan* **66**, 4042 (1997).
- ¹⁹ V. Popov, *J. Phys.: Condens. Matter* **7**, 1625 (1995).
- ²⁰ V. Popov, private communication.
- ²¹ H. Smolinski, C. Gros, W. Weber, U. Peucheret, G. Roth, M. Weiden and C. Geibel, *Phys. Rev. Lett.* **80**, 5164 (1998).
- ²² P. Horsch and F. Mack, *Eur. Phys. J. B* **5** , 367 (1998).
- ²³ E. Pigorsch and W. E. Steger, *Phys. Stat. Sol. (a)* **117**, K189, (1990).

FIGURES

FIG. 1. Schematic representation of the LiV_2O_5 crystal structure in the (a) (001) and (b) (010) plane.

FIG. 2. Room temperature polarized far-infrared reflectivity spectra of LiV_2O_5 single crystal for (a) $\mathbf{E}||\mathbf{a}$ and (b) $\mathbf{E}||\mathbf{b}$ polarizations. The experimental values are given by the open circles. The solid lines represent the calculated spectra obtained by fitting procedure described in the text.

FIG. 3. Room and low temperature Raman scattering spectra for all principal polarized configurations. $\lambda_L = 514.5$ nm

FIG. 4. Compatibility diagram relating the layer and crystal vibrations in LiV_2O_5 .

FIG. 5. The (aa) (solid lines) and (bb) (doted lines) polarized room temperature Raman spectra of LiV_2O_5 and NaV_2O_5 . Inset: Schematic representation of basing building blocks of Li- and Na-vanadate crystal structure.

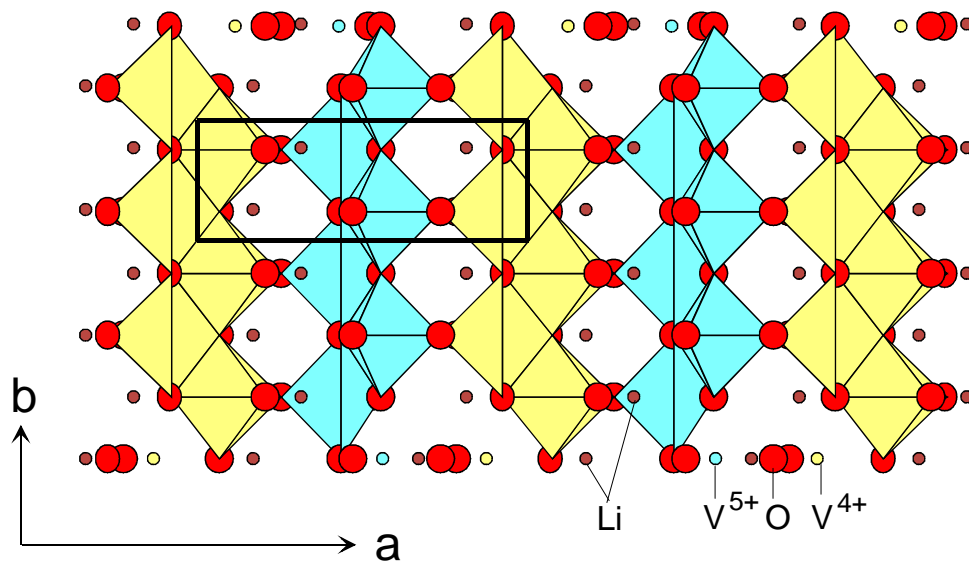
TABLES

TABLE I. Oscillator fit parameters in cm^{-1} .

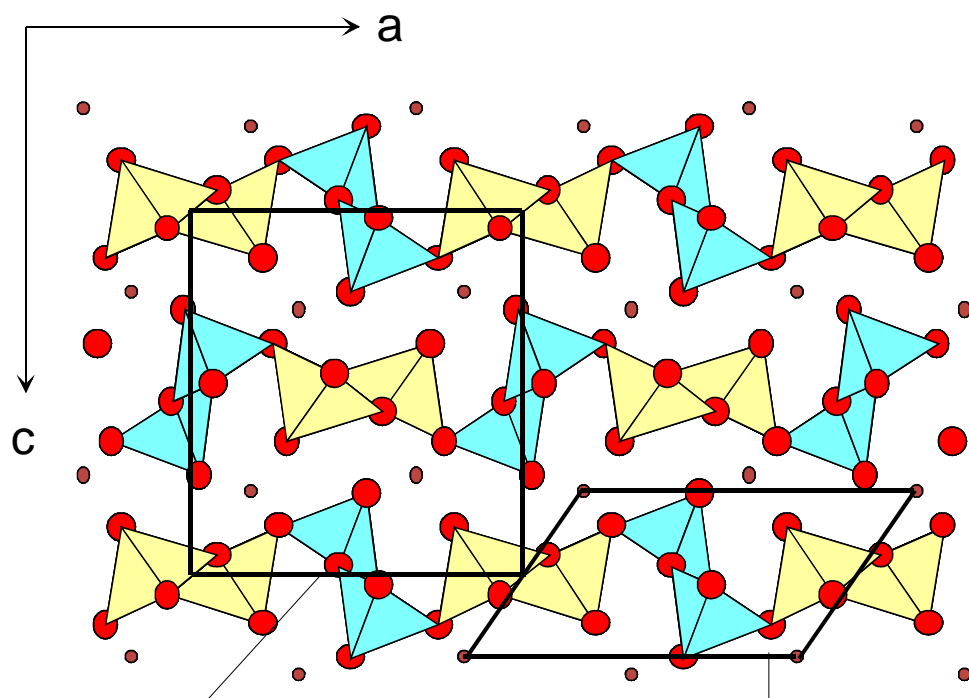
Polarization	ω_{TO}	γ_{TO}	ω_{LO}	γ_{LO}	ϵ_0	ϵ_∞	Remark
E \parallel a	202	16	230	18	16.7	6.5	Li \parallel a
	243	6	246	6			O-V-O bending
	255	7	268	23			O-V-O bending
	340	80	380	60			O-V-O bending
	397	30	402	80			$V_{1(2)} - O_1$ stretching
	545	20	622	15			$V_{1(2)} - O_{4(5)}$ stretching
	724	40	727	50			$V_1 - O_3$ stretching
	948	4	962	5			$V_2 - O_2$ stretching
	1006	4	1011	4			O-V-O bending
E \parallel b	180	25	207	35	13.4	4.5	O-V-O bending
	255	10	259	15			O-V-O bending
	323	10	350	15			$V_1 - O_1 - V_2$ bending
	557	23	571	15			$V_{1(2)} - O_1$ stretching
	595	18	790	20			$V_{1(2)} - O_{4(5)}$ stretching

TABLE II. The frequencies (in cm^{-1}) of Raman active modes of LiV_2O_5 .

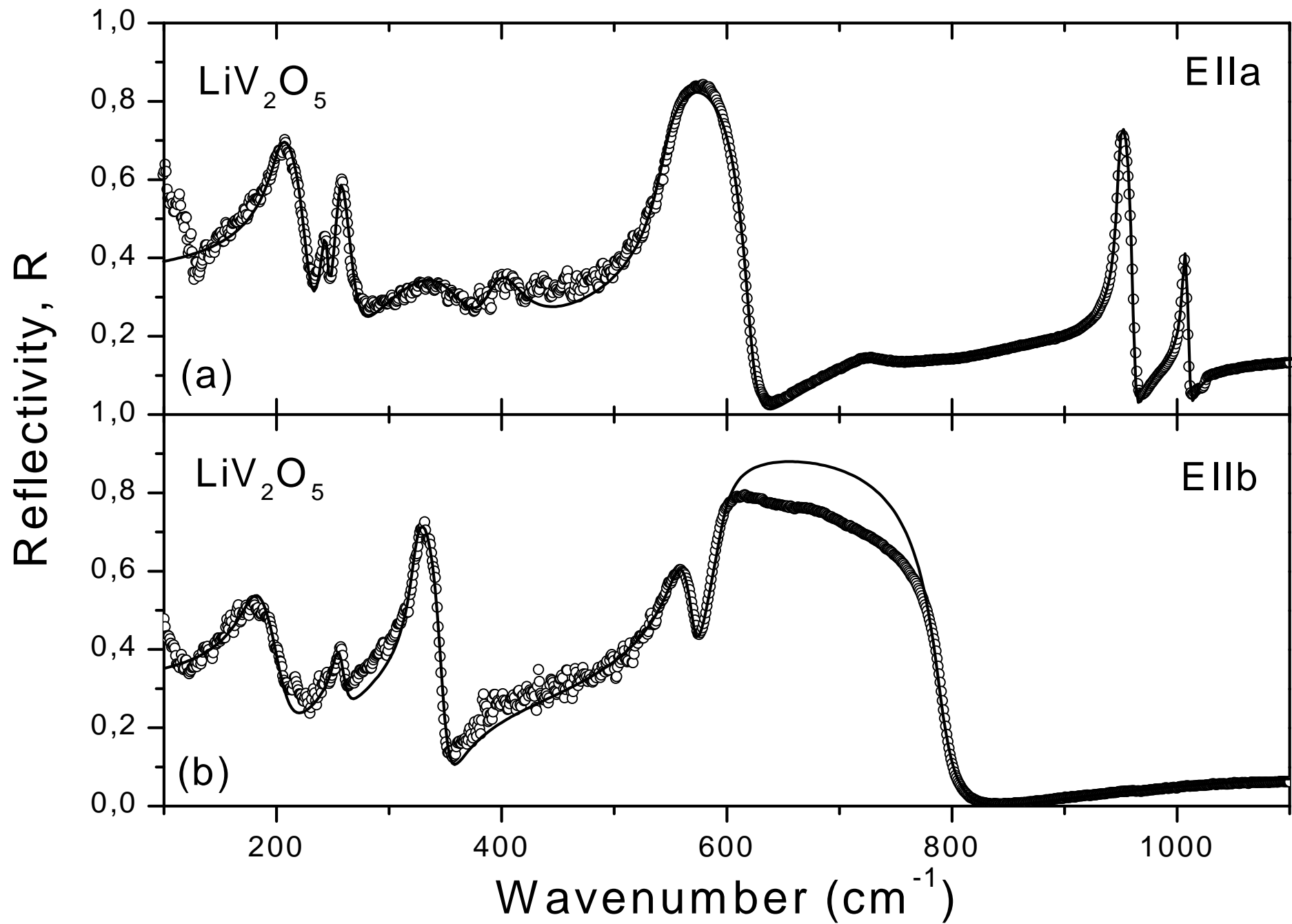
Number of peaks	A_g	B_{1g}	B_{2g}	B_{3g}
1	100	168	168	
2	123	250	250	123 A_g -2
3	172	270	270	172 A_g -3
4	197	333	333	250 B_{1g} -2
5	209	546		270 B_{1g} -3
6	267	646	646	328 A_g -7
7	328	737	737	333 B_{1g} -4
8	374			374 A_g -8
9	398			528 A_g -11
10	456			550 A_g -12
11	528			646 B_{1g} -6
12	550			737 B_{1g} -7
13	639			965 A_g -15
14	725			989 A_g -16
15	965			
16	989			

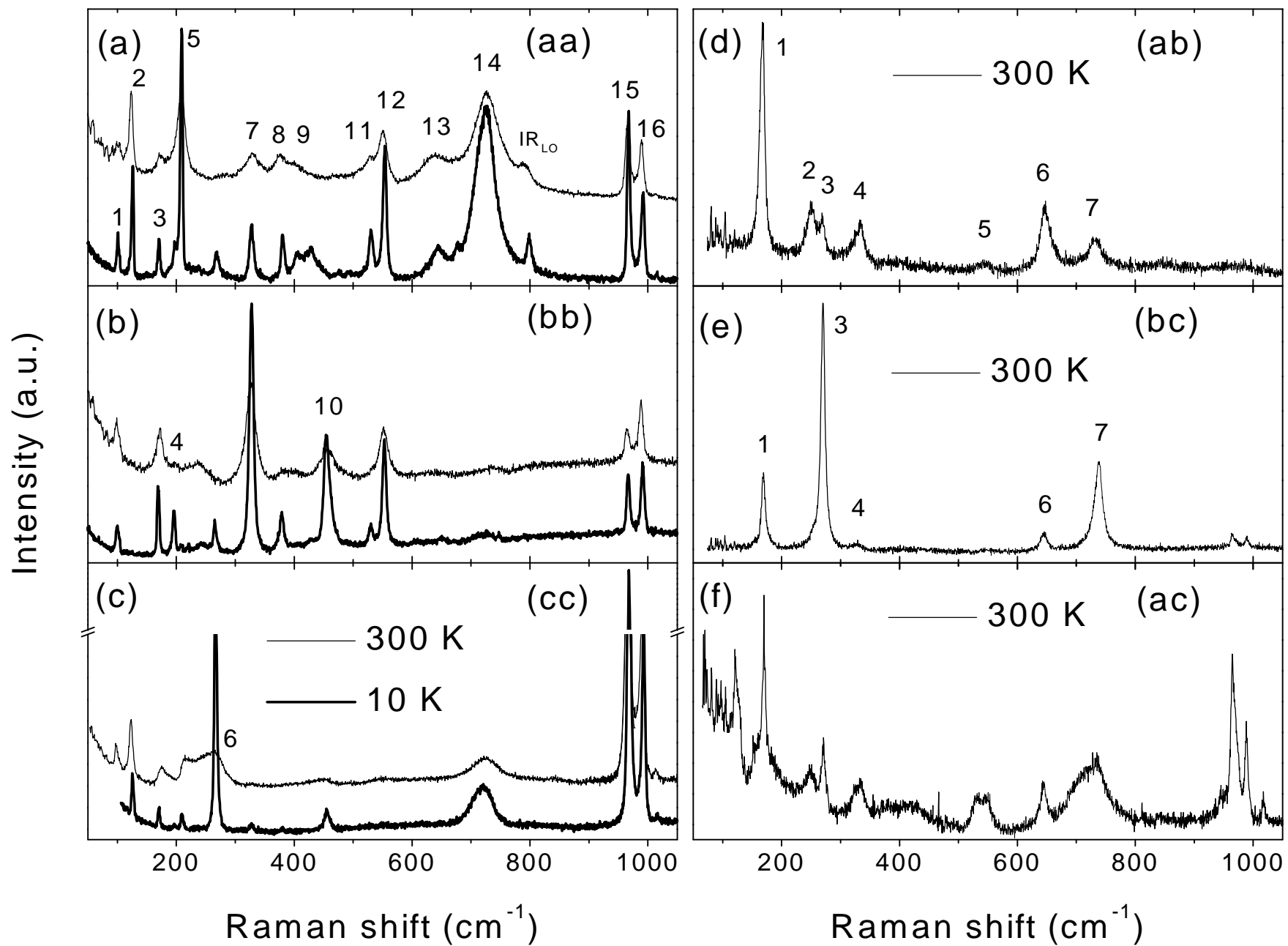


(a)



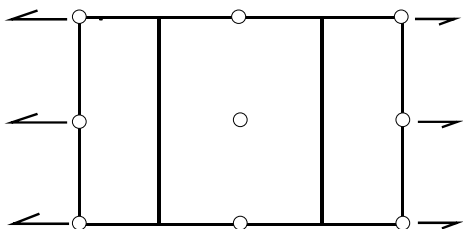
Crystal unit cell (b) Layer unit cell





Layer symmetry	Activity	Crystal symmetry	Activity
<u>16 A_g</u>	R(xx,yy,zz,xz)	<u>16 A_g</u>	R(xx,yy,zz)
<u>8 A_u</u>	IR(E y)	<u>8 A_u</u>	Silent
<u>8 B_g</u>	R(xy,yz)	<u>8 B_{1g}</u>	R(xy)
<u>16 B_u</u>	IR(E x,E z)	<u>16 B_{2g}</u>	R(xz)
		<u>8 B_{3g}</u>	R(yz)
		<u>16 B_{1u}</u>	IR(E z)
		<u>8 B_{2u}</u>	IR(E y)
		<u>16 B_{3u}</u>	IR(E x)

P1 2₁/m 1 (DG15)



P 2₁/n 2₁/m 2₁/a

